HHS Public Access

Author manuscript

Curr Eye Res. Author manuscript; available in PMC 2018 August 17.

Published in final edited form as:

Curr Eye Res. 2018 August ; 43(8): 1006–1018. doi:10.1080/02713683.2018.1464195.

In Vivo Imaging of the Retina, Choroid and Optic Nerve Head in Guinea Pigs

Ashutosh Jnawali[a,1], **Krista M Beach**[a,2], and **Lisa A Ostrin**[a,*,3]

[a]College of Optometry University of Houston, 4901 Calhoun Rd, Houston, TX 77004, USA

Abstract

Purpose—Guinea pigs are increasingly being used as a model of myopia, and may also represent a novel model of glaucoma. Here, optical coherence tomography (OCT) imaging was performed in guinea pigs. *In vivo* measurements of retinal, choroidal and optic nerve head parameters were compared with histology, and repeatability and interocular variations were assessed.

Methods—OCT imaging and histology were performed on adult guinea pigs (n = 9). Using a custom program in Matlab, total retina, ganglion cell/nerve fiber layer (GC/NFL), outer retina and choroid thicknesses were determined. Additionally, Bruch's membrane opening (BMO) area and diameter, and minimum rim width were calculated. Intraobserver, interocular and intersession coefficients of variation (CV) and intraclass correlation coefficients (ICC) were assessed.

Results—Retina, GC/NFL, outer retina and choroid thicknesses from *in vivo* OCT imaging were 147.7 ± 5.8 μm, 59.2 ± 4.5 μm, 72.4 ± 2.4 μm, and 64.8 ± 11.6 μm, respectively. Interocular CV ranged from 1.8 to 11% (paired t-test, p = 0.16 to 0.81), and intersession CV ranged from 1.1 to 5.6% (p = 0.12 to 0.82), with the choroid showing the greatest variability. BMO area was 0.192 ± 0.023 mm^2, and diameter was 493.79 ± 31.89, with intersession CV of 3.3% and 1.7%, respectively. Hyper reflective retinal layers in OCT correlated with plexiform and RPE layers in histology.

Conclusion—*In vivo* OCT imaging and quantification of guinea pig retina and optic nerve head parameters were repeatable and similar between eyes of the same animal. *In vivo* visibility of retinal cell layers correlated well with histological images.

Keywords

in vivo imaging; retina; optic nerve head; choroid; guinea pig; SD-OCT

Introduction

Myopia is associated with structural changes in the eye, including a longer axial length, thinner choroid,[1, 2] and changes in optic nerve head morphology.[3] Furthermore, myopia

*corresponding author: lostrin@central.uh.edu.
[1]AJnawali@Central.UH.EDU
[2]kbeach@Central.UH.EDU
[3]lostrin@central.uh.edu

Conflicts of interest: none

poses an increased risk for the development of primary open angle glaucoma,[4–6] which results in nerve fiber layer thinning[7] and optic nerve head changes, including decreased minimum rim width[8] and increased Bruch's membrane opening,[9] ultimately leading to permanent vision loss. Guinea pigs are becoming an increasingly popular model of myopia,[10–12] and may also represent a promising model of glaucoma. Guinea pig retinal physiology, both *in vitro* single cell recordings[13, 14] and *in vivo* electrophysiology,[15, 16] have previously been characterized. Additionally, *in vitro* retinal and optic nerve head (ONH) structures in the guinea pig have been examined;[17, 18] however, *in vivo* methods to assess the retina, choroid and ONH have not yet been established.

Optical coherence tomography (OCT) is a non-invasive imaging technique using low-coherence interferometry for cross sectional imaging of the internal tissue microstructures. OCT is widely used as an objective clinical and research tool for high resolution imaging of the retina, choroid, and ONH.[19–21] With the introduction of spectral domain (SD) OCT and eye tracking technology, high resolution scans can be obtained in a short period of time, with greater than 50,000 axial scans per second.[22–24] Studies have shown that SD-OCT has high intra- and inter-session reproducibility in monitoring glaucoma progression.[21, 25–27] OCT as a method to assess *in vivo* ocular structures in the guinea pig would be a beneficial technique to follow disease progression in this animal model.

Myopia and glaucoma have been studied in a wide variety of animal models, including dogs,[28] rats, mice,[29, 30] zebrafish[31] and non-human primates,[32] among others, which has contributed to our understanding of the disease pathology and led to innovative treatment strategies.[33, 34] However, each animal model presents unique challenges. Non-human primate models, though having a close resemblance to human anatomy and cellular organization, have limitations in terms of economics and practicality.[35] Current rodent models provide an opportunity to study genetic manipulations and test large numbers of animals, but are limited by their small globe size and structural differences in the ONH compared to humans,[33] primarily the absence of a collagenous lamina cribrosa.[36, 37] Structural changes in the lamina cribrosa have been described in glaucomatous eyes in a number of previous studies.[8, 38, 39] Unlike rats and mice, guinea pigs possess a collagenous lamina cribrosa,[17] which may be better suited to model glaucomatous change observed at the ONH in humans. Additionally, guinea pigs do not require anesthesia for intraocular pressure measurements; therefore anesthesia induced alterations in intraocular pressure can be avoided.

Another advantage of the guinea pig compared to other rodents are the similarities in retinal physiology. Unlike rats and mice which are nocturnal creatures and possess an ultraviolet sensitive cone, guinea pigs are diurnal and have short and medium wavelength cones with spectral sensitivity similar to the primate retina.[40] Guinea pig photopic electroretinogram (ERG) responses are much closer to primate photopic ERG responses than that of the rat and mouse.[15, 41] Although the guinea pig ERG has not yet been pharmacologically dissected to determine the cellular source of each waveform, its similarity to primate ERG is promising and offers potential for future studies.

Other benefits of the guinea pig include easy breeding, quick growth with developmental maturation at the age of 5 months, docile temperament, and wide availability. [42] Thus, guinea pigs, a precocial mammal frequently used as a model of human disease, are posed to be a valuable and informative model of both myopia and glaucoma structural and functional studies.

A number of studies have evaluated the retinal organization of guinea pigs, mainly using a histological approach.[43, 44] While *in vivo* OCT imaging in mice[45] and rats[46, 47] has been validated, few studies have utilized this technique in guinea pigs. Most recently, Li, et al, used OCT to assess retinal and choroidal thickness in guinea pigs to correlate axial length and refraction, and to compare to histological sections.[48] The authors reported good agreement between *in vivo* and histological measurements; however, transverse scaling was not accounted for, and only a single point in the posterior pole was assessed. Other retinal and ONH metrics, such as nerve fiber layer thickness, Bruch's membrane opening, and minimum rim width have not been evaluated in guinea pigs. Quantification of such parameters in normal guinea pigs is critical in characterizing structural changes which are expected to occur in conditions such as myopia and glaucoma. The goal of this study was to establish protocols for *in vivo* OCT imaging in the guinea pig and to characterize normal retinal, choroidal, and ONH structures. To this aim, we assessed intraobserver, interocular and intersession differences in normal guinea pigs, and compared *in vivo* images to histological analysis.

Materials and Methods

Nine adult pigmented guinea pigs of Elm Hill breed (Elm Hill Labs, MA, USA), aged 2.5 years, were included in this study (6 female, 3 male). The mean weight of males was 1151.75 ± 163.65 g and that of females was 1070.5 ± 71.28 g. Animals were kept under 12 hour light/dark cycle and provided food and water *ad libitum*. Procedures were approved by the Institutional Animal Care and Use Committee at the University of Houston and conformed to the ARVO statement for the Use of Animals in Ophthalmic and Vision Research.

Animal preparation

For imaging, animals were anesthetized with a subcutaneous injection of ketamine (30 mg/kg, VEDCO Inc, MO USA) and xylazine (3 mg/kg, Lloyd Laboratories, Philippines). Both eyes were dilated with topically instilled 2.5% tropicamide (Bauch and Lomb, NY USA) and 1% phenylephrine (Paragon BioTeck Inc, OR USA). The eyelids were held open with a custom lid speculum. To prevent the corneal surface from drying and to optimize optical quality, custom contact lenses were fabricated in-house (DAC 2X-ALM OTT, DAC International, CA USA) with Boston XO material, and inserted with artificial tears (Refresh Liquigel, Allergan). Contact lens parameters included a 3.5 mm central thickness, 8 mm total diameter, and 4.5 mm base curve.

Image Acquisition

In vivo imaging was performed for both eyes of each animal with spectral domain optical coherence tomography (SD-OCT, Spectralis HRA+OCT; Heidelberg Engineering, Heidelberg, Germany) with an 870 nm (average) super luminescent diode light source. High resolution imaging mode was utilized with an acquisition rate of 38,400 a-scans per second. The axial resolution of the instrument is 3.5 μm/pixel digital (7 μm optical) and lateral resolution of 6 μm/pixel digital (14 μm optical). Animals were positioned prone on a custom-built stage, and the instrument was aligned with the eye using the x-y-z adjustment of the camera. The posterior segment was brought into focus by first adjusting the instrument's focus and then adjusting the reference arm to bring the retinal surface into sharp focus. The mean scan focus was −3.77 ± 2.20 D for OD and −3.61 ± 1.78 D for OS. The imaging focus was similar across two eyes and across imaging sessions. Scan parameters included a 12° circular scan (1536 a-scans, Figure 1A) and a 24 line radial scan (20°, 1024 a-scans per line, 7.5° intervals, Figure 1B), both centered on the optic nerve head (ONH). Enhanced depth imaging mode was utilized for improved visualization of the choroid. Preliminary imaging showed that averaging 40 frames for circular scans and 16 frames for radial scans provided optimum noise reduction and image quality, and was therefore used for image acquisition. All images had image quality above 25 dB (mean 29 ± 2.75 dB). Approximately one week after the initial session, imaging was repeated in one eye for all animals. To minimize scan distance as a confounding factor, the contact lens, the scan focus, and the reference arm length were kept constant for each eye of each animal.

Refraction and Biometry

Refractive error was measured for each eye with animals awake, hand held, and undilated. Streak retinoscopy (WelchAllyn, Skaneateles Falls, NY, USA) was performed twice and averaged. Biometry (LenStar, Haag-Streit, Germany) was performed under anesthesia. A lid speculum was inserted, and animals were positioned on a custom stage aligned with the instrument. The LenStar biometer uses optical low coherence reflectometry to determine corneal thickness, anterior chamber depth, lens thickness and axial length. Although LenStar is calibrated for measurement of ocular dimensions in human eyes, its use has been reported in much smaller eyes such as tree shrews,[49, 50] and as reported in these studies, the ocular dimensions of tree shrews are comparable to guinea pig eyes. Since guinea pig eyes are much smaller than human eyes, the short eye mode in the biometer was used so that consistent peaks for the four refractive surfaces (cornea, anterior and posterior lens and retina) were visible (Figure 2A). Axial length and lens thickness were measured for 8 eyes against a rule following enucleation (Figures 2B, 2C). To further confirm measurements obtained from Lenstar, ocular dimensions of two eyes were compared from the LenStar and A-scan ultrasonography (AXIS II, Quantel Medical, Bozeman, MT) using immersion technique with 10 scans per eye at a frequency of 11 MHz. The media velocities for anterior chamber (1540 m/s), vitreous chamber (1540 m/s), and lens (1645 m/s) were obtained from literature.[42, 51] Corneal refractive index and lens refractive index were obtained from published normative data for guinea pigs.[42, 51] Ocular dimensions from LenStar were compared to results from A-scan ultrasonography.

Image analysis

SD-OCT images were exported as raw (.vol) files. A custom program (MatLab, MathWorks) was used to optimize the image quality, scale the images to adjust for lateral magnification, and manually segment the images. To compensate for the transverse scaling, biometric measurements were used to create a three-surface schematic eye of the guinea pig to locate the posterior nodal point,[52] and calculate the distance from the posterior nodal point to the retina (i.e. posterior nodal distance, PND). We adopted the methods for scaling calculation described previously for a three surface schematic eye.[53] Assuming a spherical globe and retina to convert linear distance of PND to angular measure in microns per degree, the PND was used to calculate the scan length and transverse scaling. The assumption that the retina is spherical helps to convert the linear distance of posterior nodal point to the retina in angular distance in microns per degree, from the relationship of length of arc and radius in a spherical surface. This method of calculating the retinal magnification factor using posterior nodal point location has been described in detail in the literature.[54, 55] The microns per degree retinal scaling (RS) was calculated as $\mathrm{RS} = \frac{\Pi}{180} \times \mathrm{PND}$. The transverse scaling (TS) in microns per pixel were calculated as TS = (microns per degree)/(pixels per degree), and this value was used as the transverse scaling factor to account for lateral magnification. After calculating the transverse scaling, each OCT B-scan image was compensated so as to maintain the same size for the length and width of each pixel, which would give the corrected measurements in three dimensions. The perpendicular direction concerned with axial scaling is based on refractive index and interference in the different components of ocular media. As such, the axial scaling was taken as 3.87 μm/pixel from the manufacturer's instructions. Figure 3 shows an image before and after scaling.

For internal limiting membrane (ILM) and Bruch's membrane, the segmentation lines were automatically delineated, and lines were manually corrected for any segmentation errors. The points on the x and y axis were interpolated for nearest neighbor while fitting the line. For other layers, a line was plotted at the 0 y position on the image and modified manually to delineate the layer of interest. For circular and radial scans, the ILM, ganglion cell/nerve fiber layer (GC/NFL), outer plexiform layer (OPL), Bruch's membrane and posterior choroid were segmented to calculate thicknesses of GC/NFL, outer retina, total retina and choroid (Figures 4A, 4B). Thicknesses were calculated for each of the 1536 a-scans of the circular scan and 1024 a-scans of each of the 24 line radial scans. For radial scans, Bruch's membrane opening (BMO) was manually identified for each line scan. The perpendicular distance from each of BMO point to the ILM was defined as minimum rim width (MRW). For BMO metrics, an ellipse was fitted through the 48 BMO points, and the area and diameter were calculated. Thickness maps were generated for total retina, GC/NFL, outer retina and choroid with the method of interpolation in Matlab, interpolating all points between the 20 degree line scans. The ONH region was excluded by applying a mask calculated from the BMO diameter. The remaining thickness map was divided into quadrants (superior, inferior, nasal and temporal) for sectoral thickness calculations.

Intraobserver, interocular, and intersession repeatability

To assess intraobserver repeatability, the image segmentation was repeated by the same observer (author AJ) on two separate occasions for one eye for each animal. For interocular comparisons, all measurements were compared between two eyes of each animal. For intersession repeatability, imaging was repeated in all animals at least a week after the first session.

Histology

Histology was performed on 7 eyes of 7 guinea pigs after OCT imaging. Animals were euthanized with 100 mg/kg sodium pentobarbital (Fatal-Plus, Vortech Pharmaceuticals, MI, USA). Eyes were marked for orientation, enucleated and bisected at the equator. Posterior segments were frozen (n = 6) or embedded in paraffin (n =1). For frozen sections, tissue was fixed overnight at 4° C in a solution of 4% paraformaldehyde in 0.1M sodium phosphate buffer, and cryoprotected in successive sucrose infiltrations (5–20%) for 6 hours. Tissue was then embedded in a 1:1 solution of 20% sucrose and optimal cutting temperature freezing compound (Tissue-Tek) and snap frozen in liquid nitrogen. Orientation markings were made on the tissue block consistent with the orientation markings of the globe. Eight μm cryosections (Leica CM 1950, Leica) were cut from the posterior segment of the eye through the ONH. With the help of orientation markings, the sections were cut through the ONH in the horizontal dimension thus extending from nasal to temporal retina. For paraffin embedding, the posterior segment was fixed overnight in 4% paraformaldehyde, dehydrated and paraffin infiltrated. Following sectioning, the slides were de-paraffinized with xylene and rehydrated. Frozen and paraffin embedded sections were stained with hematoxylin and eosin (H & E), mounted (Cytoseal 60, Richard-Allan), and imaged with a light microscope (DM1000, Leica, Germany). To be consistent with the radial scan findings from OCT imaging, three histological sections closest to the center of the ONH were used for analysis. Images were imported into Matlab and analyzed similar to OCT imaging, with manual segmentation of the ILM, Bruch's membrane, GC/NFL, and inner and outer plexiform layers for thickness calculations. Histological sections were taken through the ONH horizontally from nasal to temporal retina to avoid the visual streak, which is reportedly in the superior retina above the ONH.[43] Hyper-reflective features of the OCT images were aligned with histological images to assess correspondence of retinal and choroidal layers.

Data analysis

Data are expressed as mean ± standard deviation. Regional variations were assessed with one-way ANOVA with post-hoc Tukey-Kramer test for pairwise comparisons. The coefficient of variation (CV), intraclass correlation coefficient (ICC)[56] and 95% confidence intervals were calculated for intraobserver, interocular and intersession measures, and paired t-tests and Bland-Altman analyses[57] were performed. Statistical analysis was performed using MedCalc (MedCalc Software, 12.3.0, Mariakerke, Belgium). A critical value < 0.05 was considered statistically significant.

Results

Animals were hyperopic, with a mean spherical equivalent refraction of +3.50 ± 0.77 D. Mean axial length was 9.997 ± 0.12 mm, and mean corneal power was 71.09 ± 2.85 D. There were no statistically significant differences between the right and left eyes for refractive and biometric measures (Table 1).

For 8 eyes that were measured *in vivo* with the LenStar and subsequently enucleated and measured against a scale, average *in vivo* lens thickness and axial length were 5.34 ± 0.04 mm and 10.00 ± 0.07 mm, respectively, and *ex vivo* isolated lens thickness and axial length were 5.52 ± 0.12mm and 10.70 ± 0.39 mm. The LenStar measures axial length from the cornea to the retinal pigment epithelium, whereas *ex vivo* axial length was measured from the cornea to the sclera, so also includes the choroid and sclera. The guinea pig sclera is reported to be around 200 μm.[58] Thus, the LenStar axial length measurements are expected to be shorter than *ex vivo* measurements. Additionally, the isolated eye is no longer restrained by extraocular muscles within the orbit and therefore, small increases in length are expected after enucleation. The isolated lens is no longer stretched by zonular fibers, and therefore lens thickness is expected to be slightly different *ex vivo* compared to *in vivo*. For two additional eyes in which the ocular dimensions were measured with the LenStar and A-scan ultrasonography, axial dimensions corresponded well (shown in the representative figure S1 in the supplemental material).

From OCT images, mean total retinal thickness was 151.13 ± 6.38 μm, GC/NFL thickness was 40.39 ± 2.53 μm, outer retinal thickness was 68.32 ± 2.75 and choroidal thickness was 71.36 ± 8.57 μm. A representative example of the ILM and BMO delineation is shown in figure 5. Minimum rim width was 139.34 ± 17.17 μm, BMO area was 0.192 ± 0.023 mm^2, and BMO diameter was 489.66 ± 16.24 μm. Rim volume was 0.0126 ± 0.0022 mm^3.

Regional variations

Thicknesses for total retina, GC/NFL, outer retina and choroid by quadrant are shown in Figure 6. One-way ANOVA showed that there were significant regional variations for total retinal thickness ($F_{3,32}$ = 5.17, p = 0.005), GC/NFL ($F_{3,32}$ = 17.91, p < 0.001), and outer retina ($F_{3,32}$= 13.43, p < 0.001). Post-hoc Tukey-Kramer pairwise comparisons showed that total retina thickness was greatest in the superior region (158.29 ± 5.59 μm) and least in the inferior region (149.8 ± 4.81 μm). The GC/NFL was thinnest in the superior region (39.14 ± 2.71 μm) and thickest in the inferior region (49.12 ± 3.75 μm). The outer retina was thickest in the superior region (72.91 ± 3.20 μm) and thinnest in the inferior region (63.32 ± 2.87 μm). There were no significant nasal/temporal variations with any retinal thickness measure. There were no significant regional variations observed in the choroid ($F_{3,32}$= 0.53, p = 0.67).

Intraobserver, interocular, and intersession repeatability

Intraobserver repeatability was assessed for thicknesses of total retina, GC/NFL, outer retina and choroid, and ONH parameters by having the same observer segment the OCT images on two occasions (Table 2). Significant differences were observed for total retina, GC/NFL and

choroid; however, these differences from repeat segmentation ranged from 0.56 to 6.05 μm, which are not expected to be clinically significant. The ICCs for these measures ranged from 0.83 to 0.99, and CV ranged from 0.88% to 7.75%, indicating high repeatability.

For interocular measurements, one animal was excluded due to congenital structural irregularities around the optic nerve head of the right eye. For all thickness and ONH parameters, only outer retina thickness demonstrated significant interocular differences ($p = 0.02$, Table 3), with a mean difference of 1.70 μm. For thickness measures, interocular ICCs ranged from 0.62 to 0.93 with CVs of 2.35% to 11.76%. For ONH parameters, ICCs ranged from 0.42 to 0.69 with CVs of 4.02% to 11.40%. Overall, these results indicate that the two eyes of each animal were correlated.

Intersession measurements showed high repeatability, with no parameters demonstrating a significant intersession difference (Table 4). For thickness measures, ICCs ranged from 0.93 to 0.97 with CVs of 0.90% to 4.17%. For ONH parameters, ICCs ranged from 0.44 to 0.90, with CVs of 4.96% to 10.23%. Bland-Altman analysis is shown for total retina, GC/NFL, outer retina and choroid thickness, and MRW and BMO diameter in Figure 7.

In vivo versus histological measurements

Histological sections showed that all retinal layers were visible in the OCT image (Figure 8). Hyper-reflective regions of the OCT images corresponded to the RPE, inner/outer segment junction, outer plexiform layer, inner plexiform layer, and nerve fiber layer. OCT and histological thickness measurements are shown in Table 5. Total retinal thickness measured from histological images was 140.41 ± 10.57, which was not significantly different than that from the OCT images of the same eyes, at 151.17 ± 8.16 (paired t-test, $p = 0.11$). The GC/NFL, outer retinal, and choroid thickness were also not significantly different between *in vivo* and *in vitro* measures ($p > 0.05$ for all).

Discussion

The main goals of this study were to demonstrate the feasibility of *in vivo* imaging in guinea pigs with OCT, assess the repeatability, and compare findings with histology. Our results show that *in vivo* imaging demonstrates high repeatability within and between imaging sessions. Findings were similar between eyes of the same animal. We successfully quantified ONH parameters, including minimum rim width and BMO area, which will be important in future studies assessing effects of experimental glaucoma, as well as assessing potential structural changes in experimental myopia.

We used the LenStar biometer to determine axial dimensions of the guinea pig eye to calculate transverse magnification of the OCT images. Although LenStar is calibrated for measuring axial dimensions in human eyes, its use for measurement of axial dimensions has been previously reported in smaller eyes, including those of tree shrews, which have ocular dimensions similar to that of guinea pigs.[49, 50] In the chick eye, Penha, et al, report high correlation for anterior chamber depth, vitreous chamber depth, and axial length, with only a 0.5 mm difference in axial length between A-scan ultrasound and optical low-coherence tomography.[59] Here, we measured enucleated globes and isolated lenses against a ruler

under a dissecting microscope, and found the measurements were similar to those from the LenStar. However, enucleated tissue may be subject to deformation. Therefore, we also compared the ocular dimensions of the guinea pig eye from the LenStar with A-scan ultrasonography using immersion technique for two additional eyes, and found that measurements between ultrasound and the LenStar corresponded well.

The refractive indices for schematic eye calculations were derived using Abbe refractometer[51] which generally uses the standard wavelength of 589 nm, although the latest models allow use of wavelength other than 589 nm. We assume that the standard wavelength was used for refractive index calculation, though this is not specified. Since the central wavelength used in the Spectralis in our experiments is 870 nm, we can expect some small difference in the refractive indices of different media when compared to the literature. In rat eye, the refractive indices of different ocular components have previously been evaluated across the visible spectrum.[60] The authors demonstrated a change in refractive index of the ocular components by approximately 0.02 across the visible spectrum, which suggests that although the index does change with wavelength, the change is small. In the same paper, the authors also demonstrated that the posterior nodal distance (PND) has a trivial variation across the visible spectrum (3°), which suggests that the difference in wavelength used to calculate the refractive index and the one used in OCT should be negligible in the calculations for ocular magnification and image compensation.

It is important to evaluate whether OCT accurately reflects the true measure of the anatomy. In humans, non-human primates and rats, *in vivo* OCT imaging of retinal and ONH morphology has been found to correspond well with histology.[19, 61, 62] Here, reflective features in OCT images corresponded to plexiform and RPE layers, while dark regions corresponded to nuclear layers. Though histological thickness measurements have historically been the gold standard for tissue structure studies, histological preparation alters tissue thickness with shrinkage during fixation and expansion during rehydration. Shrinkage can occur unevenly across a given sample because of differing protein content between different cell types. We were unable to validate the thickness measurements from OCT imaging with histological sectioning as our histological sections showed variable tissue behavior (shrinkage/expansion/detachment) between the retinal layers. Studies show that fixed retinal tissue tends to undergo shrinkage, with the retinal nerve fiber layer least susceptible to shrinking, likely accounting for observed differences between our *in vivo* and histological measurements.[63]

The retinal NFL thickness is an important clinical diagnostic measure in glaucoma.[64] Decreased thickness of the NFL and alterations in ONH parameters, including minimum rim width and BMO area, have been observed in human glaucoma subjects using SD-OCT.[26, 65] Similar results have been shown in non-human primates,[66] mice,[67] and rats.[68] We demonstrated that the retinal ganglion cell/NFL thickness can be assessed with good repeatability using SD-OCT in guinea pigs, with an intraclass correlation coefficient of greater than 0.9 for intraobserver and intersession measurements.

Unlike rats and mice, guinea pigs have an avascular inner retina, with blood supply provided by the choroid. Avascular retinae that wholly depend on choroidal blood supply are

generally thinner than their intrinsically vascular counterparts.[69] In accordance with this, we found that the guinea pig retinal thickness, at about 152 μm, is less than what has been reported in rats (242 μm),[47] and in mice (175 μm).[70] Similar results have been shown between vascular and avascular retinal thickness with retinal whole mounts.[69] The choroid, on the other hand was shown to be relatively thicker in guinea pigs, at about 70 μm, while reported to be extremely thin in normal rats, at approximately 10 μm.[71] The increased thickness of the guinea pig choroid potentially compensates for the absence of an inner retinal vascular supply.

Guinea pigs possess a visual streak, analogous to an area centralis in chicks[72] or fovea in primates,[73] which has a higher density of cells. In histological preparations, Choudhury reported a higher density of ganglion cells distributed in a nasal/temporal isodensity orientation inferior to the optic nerve head.[44] Conversely, other studies have reported a higher density of ganglion cells superior to the optic nerve head, within 1–2 mm above the ONH.[43, 74] With OCT imaging, we found greater retinal thickness superior to the optic nerve head. Specifically, this was due to an increased thickness of the outer retinal layer, suggesting a higher density of photoreceptors in this region. The 20 degrees scans centered on the ONH, utilized here, and extended approximately 1 mm in the superior retina. Thus, it is likely that the radial scans captured the region of visual streak. Further studies localizing the visual streak in guinea pigs, both *in vivo* and *in vitro*, will help to understand these observed regional variations. Because the guinea pig lacks a fovea, the pattern of arcuate field loss observed in humans with glaucomatous field damage might not be expected to occur in guinea pigs, similar to other rodent models of glaucoma. However, the many other similarities between human and guinea pig retinal and ONH structure discussed here still contribute to the guinea pig being a viable model of glaucoma.

Our findings for retinal thickness (153.04 ± 7.5 μm) are comparable to those in previous studies of guinea pigs using OCT imaging, which reported retinal thicknesses of 142.17± 10.5 μm (3 mm from ONH), and 129 ± 1.3 μm (unspecified location).[48, 75] However, our measured choroidal thickness of 79.01 ± 13.43 μm is thinner than in both studies, which reported 120.9 ± 3.6 μm and 134.20 ± 16.22 μm. These differences in choroidal thickness could be due to the location that was sampled. Our measurements were derived from a 20 degree region surrounding the ONH, covering a region of about 1 mm on either side of the ONH, whereas the previous study measured the choroid 3 mm from the ONH (the location in the other study was unspecified). Our OCT images show that choroidal thickness increases with distance from the ONH, as evident in the thickness maps in Figure 6, which could explain the observed differences in choroid thickness between studies. Another potential source for variations between studies could be differences in the methods used for compensation of images during the analysis. Other possibilities that could account for differences between studies include guinea pig breed, age, OCT instrumentation, and image analysis methods. The guinea pigs used in this study were of Elm Hill breed and were 2.5 years old whereas those used in earlier studies were 5–6 weeks old and of unspecified strain.[48]

Our results show greater variability of choroidal thickness across different imaging sessions compared to retinal thickness. The choroid is known to be a highly dynamic structure with

variability in thickness resulting from a number of causes, including normal diurnal variation, use of dilating drops like tropicamide, water intake, and level of anesthesia. In our study, time of the day for repeat imaging was not controlled for; therefore, diurnal variation may have contributed to the variability in choroidal thickness. While not statistically different, the minimum rim width also demonstrated greater variability across imaging sessions compared to other parameters. The variability was likely due to difficulty in delineating the ILM at the ONH due to the protruding vascular tuft in some animals.

In OCT images, we were unable to reliably visualize the anterior lamina cribrosa surface, likely due to the thick nerve fiber layer and vascular sheath obscuring the ONH and decreasing the penetrance of the scanning laser. Using swept source OCT and additional image enhancement techniques may improve the image quality for lamina cribrosa evaluation in guinea pigs, but that has yet to be demonstrated. However, presence of a distinct, collagenous lamina cribrosa in guinea pigs has been reported in a previous study using histological approaches.[17]

A limitation in imaging the guinea pig retina is the lack of retinal vasculature as a landmark, which is a disadvantage when attempting to identify the same retinal location over repeated sessions. The optic nerve head is the only clear structure visible in the fundus image. Scans were centered over the ONH, and positional rotation might be present from one session or one eye to another, which likely accounted for some variability observed here in intersession and interocular measurements. However, there are other prominent landmarks in the guinea pig retina, like vertical and horizontal streaks, which are also prominent around the ONH, and are likely the underlying choroidal vasculature seen through the thin avascular retina. The follow up mode from Heidelberg was used for repeated imaging, and the system appeared to track locations through these landmarks, as the scan tilts changed with eye positioning in follow-up scans, and the B-scan images for radial and circular scans were similar across sessions. Heidelberg states that it employs TruTrack eye tracking in the autorescan mode for precise follow up of retinal locations across imaging sessions; however, it is unclear which retinal landmarks are utilized by the instrument. While the lack of vasculature can make it difficult to identify precise locations in the retina, it can also be an advantage to isolate disease mechanisms that are nonvasculature in nature. Additionally, the absence of inner retinal vasculature allows direct measurements of the nerve fiber layer without requiring mathematical subtraction of the vessels. Another limitation in our study was the lack of cycloplegia during refraction measurements. Guinea pigs have an accommodative amplitude of approximately 5 diopters.[76] However, they have been shown to demonstrate a poor voluntary accommodative response,[77] and therefore, we do not expect the lack of cycloplegia to have a significant effect on refraction measurements. Another limitation was variations in time of day for OCT imaging, which might have contributed to observed variability in choroidal thickness measurements between animals and between sessions. The extent to which the guinea pig choroid undergoes diurnal thickness changes has yet to be investigated. Finally, variability between our *in vivo* and histological measurements could have been from tissue shrinkage and other structural changes that occur during processing.

In conclusion, we demonstrated that high quality retinal imaging and *in vivo* characterization of guinea pig retina, and ONH are repeatable and in close agreement to histological measurements. Such *in vivo* imaging in guinea pigs has potential benefits in myopia and glaucoma studies in this animal model.

Supplementary Material

Refer to Web version on PubMed Central for supplementary material.

Acknowledgments

Funding: The work was supported by NIH NEI K08 EY022696 and NIH NEI P30 EY007551

Thanks to Nimesh Patel for help with software development, Jason Marsack for creating the custom contact lenses, Chris Kuether for constructing the custom stages, and David Calkins for helpful comments on the manuscript.

Abbreviations

ONH	optic nerve head
RGC	retinal ganglion cell
SD-OCT	spectral domain optical coherence tomography
EDI	enhanced depth imaging
MRW	minimum rim width
H & E	hematoxylin and eosin

References

1. Fontaine M, Gaucher D, Sauer A, Speeg-Schatz C. Choroidal thickness and ametropia in children: a longitudinal study. Eur J Ophthalmol. 2017
2. El-Shazly AA, Farweez YA, ElSebaay ME, El-Zawahry WMA. Correlation between choroidal thickness and degree of myopia assessed with enhanced depth imaging optical coherence tomography. Eur J Ophthalmol. 2017; 27(5):577–84. [PubMed: 28362057]
3. AttaAllah HR, Omar IAN, Abdelhalim AS. Evaluation of Optic Nerve Head Parameters and Retinal Nerve Fiber Layer Thickness in Axial Myopia Using SD OCT. Ophthalmol Ther. 2017; 6(2):335–41. [PubMed: 28584935]
4. Suzuki Y, Iwase A, Araie M, Yamamoto T, Abe H, Shirato S, et al. Risk factors for open-angle glaucoma in a Japanese population: the Tajimi Study. Ophthalmology. 2006; 113(9):1613–7. Epub 2006/07/11. [PubMed: 16828504]
5. Mitchell P, Hourihan F, Sandbach J, Wang JJ. The relationship between glaucoma and myopia: the Blue Mountains Eye Study. Ophthalmology. 1999; 106(10):2010–5. Epub 1999/10/16. [PubMed: 10519600]
6. Xu L, Wang Y, Wang S, Jonas JB. High myopia and glaucoma susceptibility the Beijing Eye Study. Ophthalmology. 2007; 114(2):216–20. Epub 2006/11/25. [PubMed: 17123613]
7. Cull GA, Reynaud J, Wang L, Cioffi GA, Burgoyne CF, Fortune B. Relationship between orbital optic nerve axon counts and retinal nerve fiber layer thickness measured by spectral domain optical coherence tomography. Invest Ophthalmol Vis Sci. 2012; 53(12):7766–73. [PubMed: 23125332]
8. Ivers KM, Sredar N, Patel NB, Rajagopalan L, Queener HM, Twa MD, et al. In Vivo Changes in Lamina Cribrosa Microarchitecture and Optic Nerve Head Structure in Early Experimental Glaucoma. PloS one. 2015; 10(7):e0134223. [PubMed: 26230993]

9. Fortune B, Reynaud J, Hardin C, Wang L, Sigal IA, Burgoyne CF. Experimental Glaucoma Causes Optic Nerve Head Neural Rim Tissue Compression: A Potentially Important Mechanism of Axon Injury. Invest Ophthalmol Vis Sci. 2016; 57(10):4403–11. [PubMed: 27564522]
10. Howlett MH, McFadden SA. Spectacle lens compensation in the pigmented guinea pig. Vision Res. 2009; 49(2):219–27. Epub 2008/11/11. [PubMed: 18992765]
11. Liu Q, Wu J, Wang X, Zeng J. Changes in muscarinic acetylcholine receptor expression in form deprivation myopia in guinea pigs. Mol Vis. 2007; 13:1234–44. Epub 2007/08/08. [PubMed: 17679952]
12. Garcia MB, Jha AK, Healy KE, Wildsoet CF. A Bioengineering Approach to Myopia Control Tested in a Guinea Pig Model. Invest Ophthalmol Vis Sci. 2017; 58(3):1875–86. [PubMed: 28358959]
13. Demb JB, Haarsma L, Freed MA, Sterling P. Functional circuitry of the retinal ganglion cell's nonlinear receptive field. J Neurosci. 1999; 19(22):9756–67. [PubMed: 10559385]
14. Zaghloul KA, Boahen K, Demb JB. Different circuits for ON and OFF retinal ganglion cells cause different contrast sensitivities. J Neurosci. 2003; 23(7):2645–54. [PubMed: 12684450]
15. Racine J, Joly S, Rufiange M, Rosolen S, Casanova C, Lachapelle P. The photopic ERG of the albino guinea pig (Cavia porcellus): a model of the human photopic ERG. Doc Ophthalmol. 2005; 110(1):67–77. [PubMed: 16249958]
16. Racine J, Behn D, Lachapelle P. Structural and functional maturation of the retina of the albino Hartley guinea pig. Doc Ophthalmol. 2008; 117(1):13–26. [PubMed: 18034273]
17. Ostrin LA. Optic nerve head and intraocular pressure in the guinea pig eye. Experimental Eye Research. 2016:7–16. [PubMed: 26698659]
18. Rodriguez-Ramos Fernandez J, Dubielzig RR. Ocular comparative anatomy of the family Rodentia. Veterinary ophthalmology. 2013; 16(Suppl 1):94–9. [PubMed: 23734597]
19. Huang D, Swanson EA, Lin CP, Schuman JS, Stinson WG, Chang W, et al. Optical coherence tomography. Science. 1991; 254(5035):1178–81. Epub 1991/11/22. [PubMed: 1957169]
20. Bussel II, Wollstein G, Schuman JS. OCT for glaucoma diagnosis, screening and detection of glaucoma progression. The British journal of ophthalmology. 2014; 98(Suppl 2):ii15–9. Epub 2013/12/21. [PubMed: 24357497]
21. Schuman JS, Pedut-Kloizman T, Hertzmark E, Hee MR, Wilkins JR, Coker JG, et al. Reproducibility of nerve fiber layer thickness measurements using optical coherence tomography. Ophthalmology. 1996; 103(11):1889–98. Epub 1996/11/01. [PubMed: 8942887]
22. Sander B, Larsen M, Thrane L, Hougaard JL, Jorgensen TM. Enhanced optical coherence tomography imaging by multiple scan averaging. The British journal of ophthalmology. 2005; 89(2):207–12. Epub 2005/01/25. [PubMed: 15665354]
23. Sakamoto A, Hangai M, Yoshimura N. Spectral-domain optical coherence tomography with multiple B-scan averaging for enhanced imaging of retinal diseases. Ophthalmology. 2008; 115(6): 1071–8e7. Epub 2007/12/07. [PubMed: 18061270]
24. Kotowski J, Wollstein G, Folio LS, Ishikawa H, Schuman JS. Clinical use of OCT in assessing glaucoma progression. Ophthalmic surgery, lasers & imaging: the official journal of the International Society for Imaging in the Eye. 2011; 42(Suppl):S6–s14. Epub 2011/07/28.
25. Lee SH, Kim SH, Kim TW, Park KH, Kim DM. Reproducibility of retinal nerve fiber thickness measurements using the test-retest function of spectral OCT/SLO in normal and glaucomatous eyes. Journal of glaucoma. 2010; 19(9):637–42. Epub 2010/02/23. [PubMed: 20173650]
26. Chauhan BC, O'Leary N, Almobarak FA, Reis AS, Yang H, Sharpe GP, et al. Enhanced detection of open-angle glaucoma with an anatomically accurate optical coherence tomography-derived neuroretinal rim parameter. Ophthalmology. 2013; 120(3):535–43. Epub 2012/12/26. [PubMed: 23265804]
27. Quigley HA, Broman AT. The number of people with glaucoma worldwide in 2010 and 2020. Br J Ophthalmol. 2006; 90(3):262–7. [PubMed: 16488940]
28. Gelatt KN, Gum GG, Gwin RM, Bromberg NM, Merideth RE, Samuelson DA. Primary open angle glaucoma: inherited primary open angle glaucoma in the beagle. Am J Pathol. 1981; 102(2):292–5. [PubMed: 7468772]

29. Sappington RM, Carlson BJ, Crish SD, Calkins DJ. The microbead occlusion model: a paradigm for induced ocular hypertension in rats and mice. Invest Ophthalmol Vis Sci. 2010; 51(1):207–16. [PubMed: 19850836]
30. Bergen MA, Park HN, Chakraborty R, Landis EG, Sidhu C, He L, et al. Altered Refractive Development in Mice With Reduced Levels of Retinal Dopamine. Invest Ophthalmol Vis Sci. 2016; 57(10):4412–9. [PubMed: 27750284]
31. Veth KN, Willer JR, Collery RF, Gray MP, Willer GB, Wagner DS, et al. Mutations in zebrafish lrp2 result in adult-onset ocular pathogenesis that models myopia and other risk factors for glaucoma. PLoS Genet. 2011; 7(2):e1001310. [PubMed: 21379331]
32. Harwerth RS, Crawford ML, Frishman LJ, Viswanathan S, Smith EL 3rd, Carter-Dawson L. Visual field defects and neural losses from experimental glaucoma. Prog Retin Eye Res. 2002; 21(1):91–125. Epub 2002/03/22. [PubMed: 11906813]
33. Rachida. Animal Models of Glaucoma. Journal of Biomedicine and Biotechnology. 2012
34. Aires ID, Ambrosio AF, Santiago AR. Modeling Human Glaucoma: Lessons from the in vitro Models. Ophthalmic Res. 2017; 57(2):77–86. Epub 2016/09/13. [PubMed: 27618367]
35. Burgoyne CF. The non-human primate experimental glaucoma model. Exp Eye Res. 2015; 141:57–73. Epub 2015/06/14. [PubMed: 26070984]
36. Dai C, Khaw PT, Yin ZQ, Li D, Raisman G, Li Y. Structural basis of glaucoma: the fortified astrocytes of the optic nerve head are the target of raised intraocular pressure. Glia. 2012; 60(1): 13–28. Epub 2011/09/29. [PubMed: 21948238]
37. Sun D, Lye-Barthel M, Masland RH, Jakobs TC. The morphology and spatial arrangement of astrocytes in the optic nerve head of the mouse. J Comp Neurol. 2009; 516(1):1–19. [PubMed: 19562764]
38. Quigley HA, Hohman RM, Addicks EM, Massof RW, Green WR. Morphologic changes in the lamina cribrosa correlated with neural loss in open angle glaucoma. Am J Ophthalmol. 1983:673–91. [PubMed: 6846459]
39. Roberts MD, Grau V, Grimm J, Reynaud J, Bellezza AJ, Burgoyne CF, Downs JC. Remodeling of the connective tissue microarchitecture of the lamina cribrosa in early experimental glaucoma. Investig Ophthalmol Vis Sci. 2009:681–90. [PubMed: 18806292]
40. Jacobs GH, Deegan JF 2nd. Spectral sensitivity, photopigments, and color vision in the guinea pig (Cavia porcellus). Behav Neurosci. 1994; 108(5):993–1004. [PubMed: 7826522]
41. Lei B. The ERG of guinea pig (Cavis porcellus): comparison with I-type monkey and E-type rat. Documenta ophthalmologica Advances in ophthalmology. 2003; 106(3):243–9. Epub 2003/05/10. [PubMed: 12737501]
42. Zhou X, Qu J, Xie R, Wang R, Jiang L, Zhao H, et al. Normal development of refractive state and ocular dimensions in guinea pigs. Vision research. 2006; 46(18):2815–23. Epub 05/26. [PubMed: 16723148]
43. Do-Nascimento JL, Do-Nascimento RS, Damasceno BA, Silveira LC. The neurons of the retinal ganglion cell layer of the guinea pig: quantitative analysis of their distribution and size. Brazilian journal of medical and biological research = Revista brasileira de pesquisas medicas e biologicas/ Sociedade Brasileira de Biofisica [et al]. 1991; 24(2):199–214.
44. Choudhury BP. Retinotopic organization of the guinea pig's visual cortex. Brain Res. 1978; 144(1): 19–29. [PubMed: 638761]
45. Gabriele ML, Ishikawa H, Schuman JS, Bilonick RA, Kim J, Kagemann L, et al. Reproducibility of spectral-domain optical coherence tomography total retinal thickness measurements in mice. Invest Ophthalmol Vis Sci. 2010; 51(12):6519–23. [PubMed: 20574022]
46. Lozano DC, Twa MD. Quantitative evaluation of factors influencing the repeatability of SD-OCT thickness measurements in the rat. Invest Ophthalmol Vis Sci. 2012; 53(13):8378–85. [PubMed: 23169883]
47. Yang JH, Yu SY, Kim TG, Seo KH, Kwak HW. Repeatability and Reproducibility of Spectral-Domain Optical Coherence Tomography Measurements of Retinal Thickness in Rats. Curr Eye Res. 2016; 41(10):1346–52. [PubMed: 26862705]

48. Li T, Zhou X, Luo X, Jiang B. Optical coherence tomography and histologic measurements of retinal and choroidal thicknesses in guinea pig eyes. Int J Clin Exp Med. 2016; 9(4):7080–7. Epub April 15, 2016.
49. Gawne TJ, Ward AH, Norton TT. Long-wavelength (red) light produces hyperopia in juvenile and adolescent tree shrews. Vision Res. 2017; 140:55–65. [PubMed: 28801261]
50. Gawne TJ, Siegwart JT Jr, Ward AH, Norton TT. The wavelength composition and temporal modulation of ambient lighting strongly affect refractive development in young tree shrews. Exp Eye Res. 2016; 155:75–84. Epub 12/17. [PubMed: 27979713]
51. Howlett MH, McFadden SA. Emmetropization and schematic eye models in developing pigmented guinea pigs. Vision Res. 2007; 47(9):1178–90. Epub 2007/03/16. [PubMed: 17360016]
52. Bennett AG. A method of determining the equivalent powers of the eye and its crystalline lens without resort to phakometry. Ophthalmic & physiological optics: the journal of the British College of Ophthalmic Opticians (Optometrists). 1988; 8(1):53–9. Epub 01/01. [PubMed: 3047630]
53. Patel NB, Luo X, Wheat JL, Harwerth RS. Retinal nerve fiber layer assessment: area versus thickness measurements from elliptical scans centered on the optic nerve. Invest Ophthalmol Vis Sci. 2011; 52(5):2477–89. Epub 01/12. [PubMed: 21220552]
54. Holden AL, Hayes BP, Fitzke FW. Retinal magnification factor at the ora terminals: a structural study of human and animal eyes. Vision research. 1987; 27(8):1229–35. Epub 01/01. [PubMed: 3424670]
55. Lapuerta P, Schein SJ. A four-surface schematic eye of macaque monkey obtained by an optical method. Vision research. 1995; 35(16):2245–54. Epub 08/01. [PubMed: 7571461]
56. Shrout PE, Fleiss JL. Intraclass correlations: uses in assessing rater reliability. Psychol Bull. 1979; 86(2):420–8. [PubMed: 18839484]
57. Bland JM, Altman DG. Statistical methods for assessing agreement between two methods of clinical measurement. Lancet. 1986; 1(8476):307–10. [PubMed: 2868172]
58. Cui D, Trier K, Zeng J, Wu K, Yu M, Hu J, et al. Effects of 7-methylxanthine on the sclera in form deprivation myopia in guinea pigs. Acta Ophthalmol. 2011; 89(4):328–34. [PubMed: 19860777]
59. Penha AM, Burkhardt E, Schaeffel F, Feldkaemper MP. Ultrasonography and optical low-coherence interferometry compared in the chicken eye. Optom Vis Sci. 2012; 89(6):916–21. [PubMed: 22561207]
60. Chaudhuri A, Hallett PE, Parker JA. Aspheric curvatures, refractive indices and chromatic aberration for the rat eye. Vision research. 1983; 23(12):1351–63. Epub 01/01. [PubMed: 6666037]
61. Schuman JS, Pedut-Kloizman T, Pakter H, Wang N, Guedes V, Huang L, et al. Optical coherence tomography and histologic measurements of nerve fiber layer thickness in normal and glaucomatous monkey eyes. Invest Ophthalmol Vis Sci. 2007; 48(8):3645–54. Epub 07/27. [PubMed: 17652734]
62. Huang L, Schuman J, Wang N. Comparison of nerve fiber layer thickness between optical coherence tomography and histomorphometry in glaucomatous monkey eyes. [Zhonghua yan ke za zhi] Chinese journal of ophthalmology. 2002; 37(3):188–92. Epub 02/28.
63. Abbott CJ, McBrien NA, Grunert U, Pianta MJ. Relationship of the optical coherence tomography signal to underlying retinal histology in the tree shrew (Tupaia belangeri). Invest Ophthalmol Vis Sci. 2009; 50(1):414–23. Epub 2008/08/19. [PubMed: 18708623]
64. Bowd C, Weinreb RN, Zangwill LM. Evaluating the optic disc and retinal nerve fiber layer in glaucoma. I: Clinical examination and photographic methods. Seminars in ophthalmology. 2000; 15(4):194–205. Epub 2007/06/26. [PubMed: 17585434]
65. Firat PG1DS, Demirel EE, Colak C. Comparison of ganglion cell and retinal nerve fiber layer thickness in primary open-angle glaucoma and normal tension glaucoma with spectral-domain OCT. Graefes Arch Clin Exp Ophthalmol. 2013:831–8. [PubMed: 22903819]
66. Fortune BCG, Reynaud J, Wang L, Burgoyne CF. Relating Retinal Ganglion Cell Function and Retinal Nerve Fiber Layer (RNFL) Retardance to Progressive Loss of RNFL Thickness and Optic Nerve Axons in Experimental Glaucoma. Invest Ophthalmol Vis Sci. 2015:3936–44. [PubMed: 26087359]

67. Nakano N1IH, Hangai M, Muraoka Y, Toda Y, Kakizuka A, Yoshimura N. Longitudinal and simultaneous imaging of retinal ganglion cells and inner retinal layers in a mouse model of glaucoma induced by N-methyl-D-aspartate. Invest Ophthalmol Vis Sci. 2011:8754–62. [PubMed: 22003119]

68. Huang XR1ZY, Kong W, Knighton RW. Reflectance decreases before thickness changes in the retinal nerve fiber layer in glaucomatous retinas. Invest Ophthalmol Vis Sci. 2011:6737–42. [PubMed: 21730345]

69. Buttery RG, Hinrichsen CF, Weller WL, Haight JR. How thick should a retina be? A comparative study of mammalian species with and without intraretinal vasculature. Vision Res. 1991; 31(2): 169–87. [PubMed: 2017880]

70. Kocaoglu OP, Uhlhorn SR, Hernandez E, Juarez RA, Will R, Parel JM, et al. Simultaneous fundus imaging and optical coherence tomography of the mouse retina. Invest Ophthalmol Vis Sci. 2007; 48(3):1283–9. Epub 02/28. [PubMed: 17325174]

71. Toyoda F, Tanaka Y, Shimmura M, Kinoshita N, Takano H, Kakehashi A. Diabetic Retinal and Choroidal Edema in SDT Rats. Journal of diabetes research. 2016; 2016:2345141. Epub 01/20. [PubMed: 26783535]

72. Straznicky C, Chehade M. The formation of the area centralis of the retinal ganglion cell layer in the chick. Development. 1987; 100(3):411–20. [PubMed: 3652978]

73. Patel NB, Hung LF, Harwerth RS. Postnatal maturation of the fovea in Macaca mulatta using optical coherence tomography. Exp Eye Res. 2017; 164:8–21. [PubMed: 28778401]

74. Cobcroft M, Vaccaro T, Mitrofanis J. Distinct patterns of distribution among NADPH-diaphorase neurones of the guinea pig retina. Neurosci Lett. 1989; 103(1):1–7. [PubMed: 2779850]

75. Lu F, Zhou X, Jiang L, Fu Y, Lai X, Xie R, et al. Axial myopia induced by hyperopic defocus in guinea pigs: A detailed assessment on susceptibility and recovery. Exp Eye Res. 2009; 89(1):101–8. Epub 2009/03/10. [PubMed: 19268468]

76. Ostrin LA, Garcia MB, Choh V, Wildsoet CF. Pharmacologically stimulated pupil and accommodative changes in Guinea pigs. Invest Ophthalmol Vis Sci. 2014; 55(8):5456–65. [PubMed: 25097245]

77. Jiang L, Schaeffel F, Zhou X, Zhang S, Jin X, Pan M, et al. Spontaneous axial myopia and emmetropization in a strain of wild-type guinea pig (Cavia porcellus). Invest Ophthalmol Vis Sci. 2009; 50(3):1013–9. Epub 2008/11/26. [PubMed: 19029033]

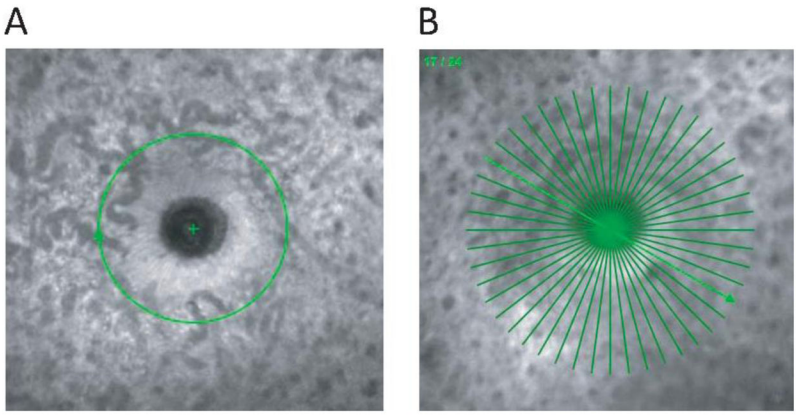

Figure 1.

A) Scanning laser ophthalmoscope image of the ONH showing the 12 degree circular scan centered on the ONH. B) Scanning laser ophthalmoscope image of the ONH showing the 20 degree, 24 line radial scan.

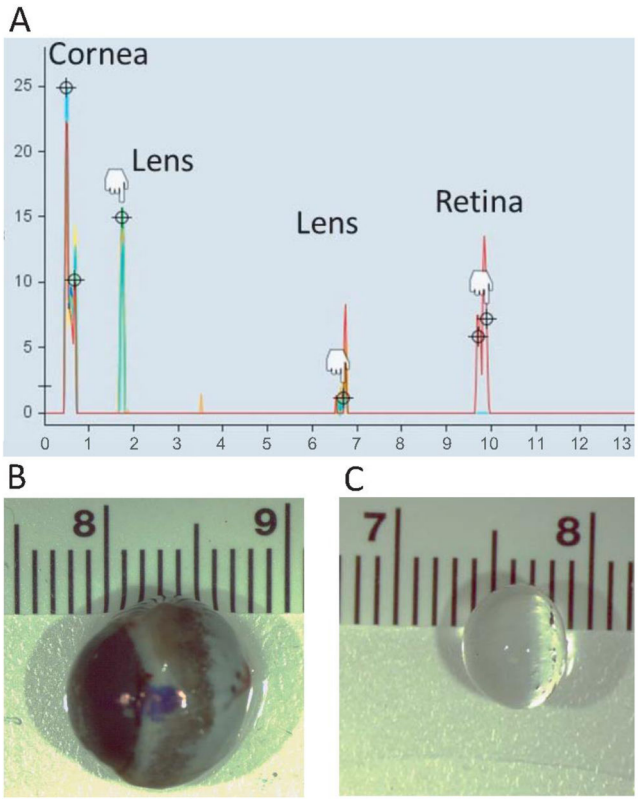

Figure 2.

A) Representative A-scan derived from the LenStar biometer from an adult guinea pig in this study. B) Enucleated globe and C) isolated lens shown against a scale (cm).

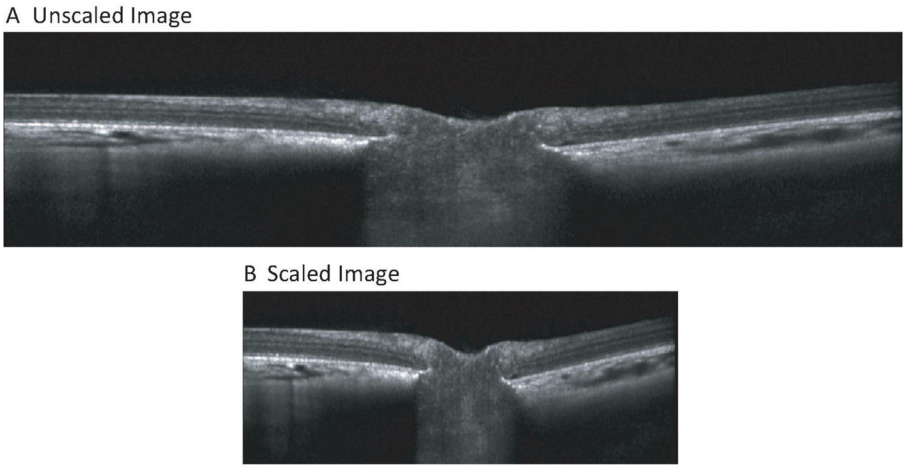

Figure 3.

A) Raw OCT image through the optic nerve head. B) Same image corrected for lateral magnification.

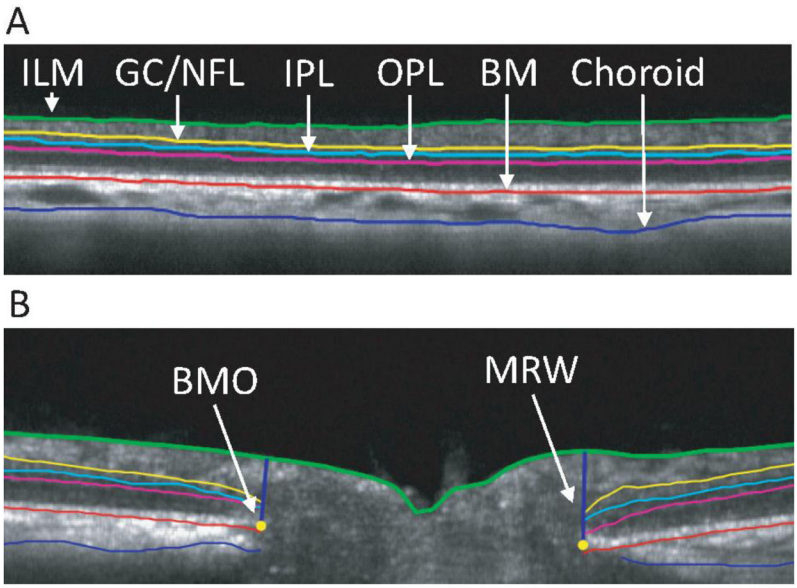

Figure 4.

A) B-scan image of 12 degree circular scan. B) B-scan image for a single line of radial scan. Segmentation indicates inner limiting membrane (ILM, green), ganglion cell/nerve fiber layer complex (GC/NFL, yellow), inner plexiform layer (IPL, light blue), outer plexiform layer (OPL, magenta), Bruch's membrane (BM, red), and posterior choroid (blue).

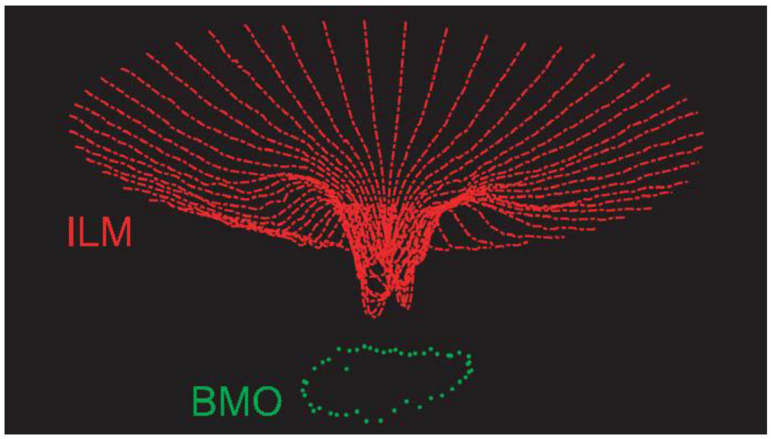

Figure 5.

A three-dimensional point cloud illustrating the inner limiting membrane (ILM, red) and Bruch's membrane opening (BMO, green) for one eye, derived from a 24 line radial scan.

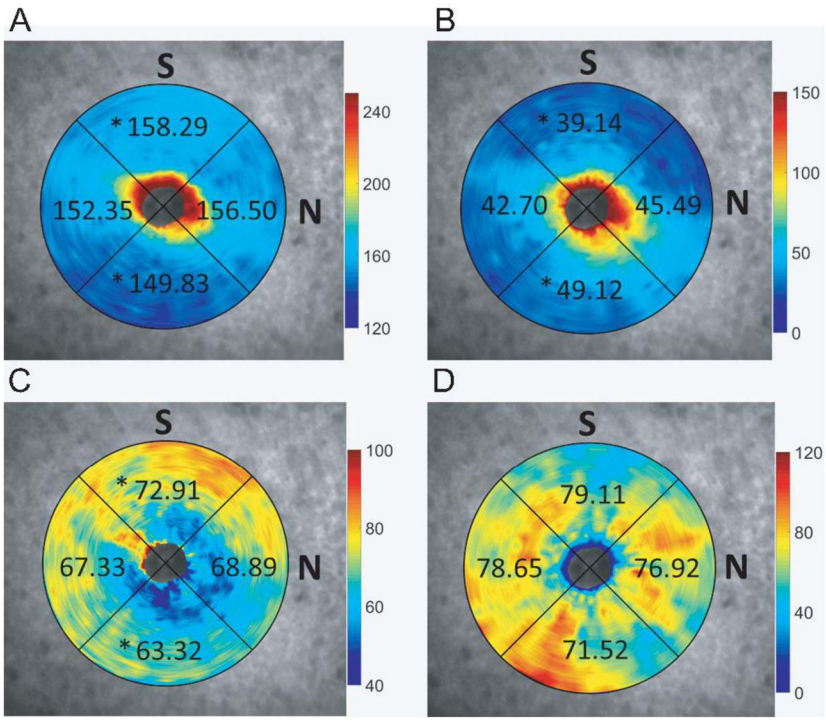

Figure 6.

Thickness maps derived from 24 line radial scans for A) total retina, B) ganglion cell/nerve fiber layer complex, C) outer retina, and D) choroid, overlaid on the corresponding scanning laser ophthalmoscope images; * indicates significant ($p < 0.05$) difference between superior and temporal thicknesses.

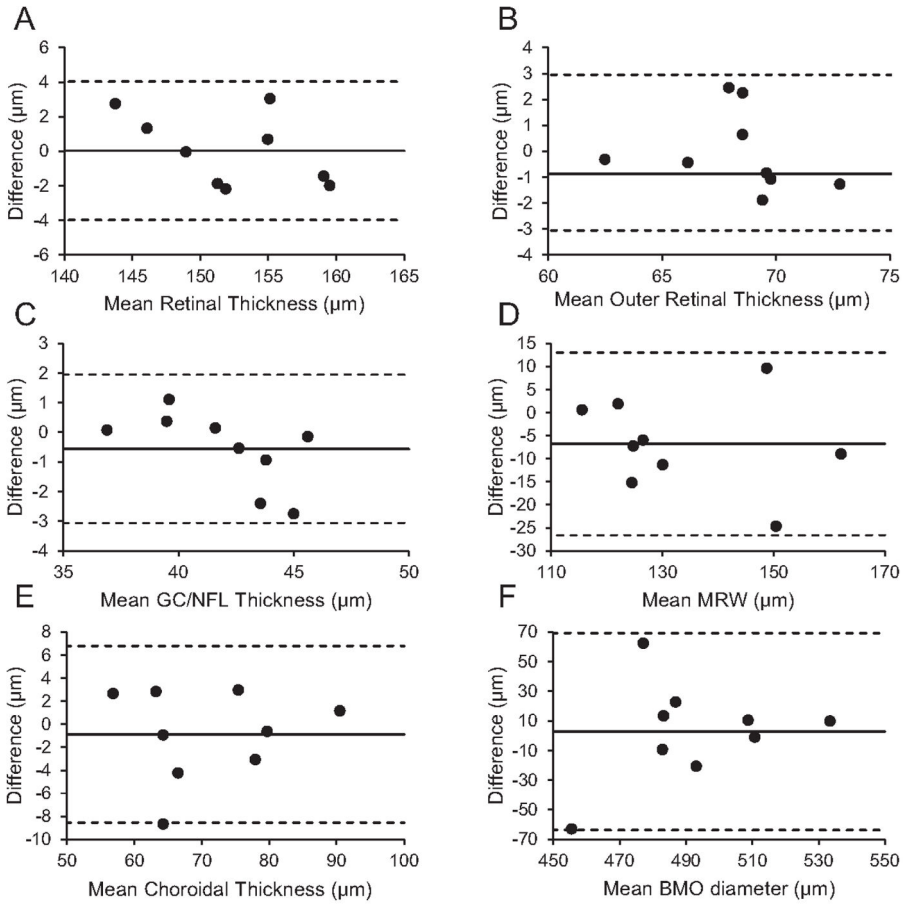

Figure 7.

Intersession Bland-Altman analysis for A) total retinal thickness, B) outer retinal thickness, C) ganglion cell/nerve fiber layer (GC/NFL) thickness, D) minimum rim width (MRW), E) choroidal thickness, and F) Bruch's membrane opening (BMO) diameter.

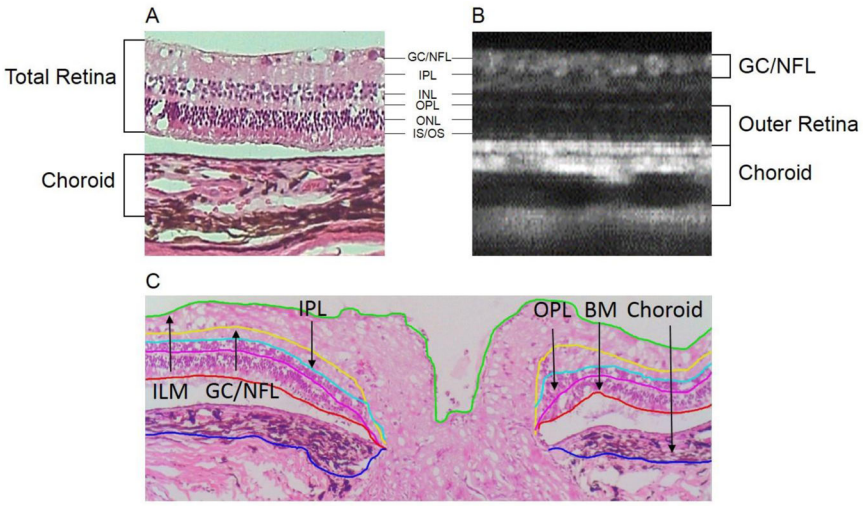

Figure 8.

A) Histological section showing tissue layers with corresponding layers in the (B) OCT b-scan. C) Segmentation of the layers in a representative histological section showing the inner plexiform layer (ILM, green), ganglion cell/nerve fiber layer complex (GC/NFL, yellow), inner plexiform layer (IPL, light blue), outer plexiform layer (OPL, magenta), Bruch's membrane (BM, red), and choroid (blue).

Table 1

Spherical equivalent refraction and biometric measurements, including central corneal thickness, anterior chamber depth, lens thickness, axial length, and mean corneal power, for right (OD) and left (OS) eyes (n = 8), compared with paired t-test

	Spherical equivalent refraction (D)	Central corneal thickness (μm)	Anterior chamber depth (mm)	Lens thickness (mm)	Axial length (mm)	Corneal power (D)
OD	+3.28 ± 0.94	251.75 ± 20.81	1.21 ± 0.09	5.52 ± 0.08	9.995 ± 0.11	72.18 ± 2.83
OS	+3.73 ± 0.55	252.5 ± 20.75	1.21 ± 0.11	5.54 ± 0.08	9.998 ± 0.13	70.00 ± 2.87
p value	0.299	0.94	0.94	0.67	0.77	0.20

Table 2

Intraobserver measures for the left eye of each animal (n = 9), measurements compared with paired t-test

	Segmentation 1	Segmentation 2	Difference	p value	ICC	95% CI	CV (%)
Total retinal thickness (μm)	152.29 ± 5.04	154.24 ± 4.85	1.95	*<0.0001	0.99	0.98 to 0.99	0.95
GC/NFL thickness (μm)	41.73 ± 2.53	44.11 ± 2.40	0.56	*<0.0001	0.97	0.88 to 0.99	4.25
Outer retinal thickness (μm)	68.32 ± 2.76	68.11 ± 2.98	0.21	0.62	0.95	0.79 to 0.99	1.24
Choroidal Thickness (μm)	70.50 ± 10.94	76.55 ± 13.46	6.05	*0.01	0.94	0.73 to 0.99	7.75
BMO area (mm^2)	0.19 ± 0.02	0.19 ± 0.02	0.002	0.13	0.98	0.91 to 0.99	1.81
BMO diameter (μm)	493.79 ± 31.89	490.76 ± 29.98	3.03	0.16	0.98	0.92 to 0.99	0.88
MRW (μm)	130.43 ± 15.63	127.16 ± 15.50	3.27	0.17	0.91	0.66 to 0.98	3.59
Rim volume (mm^3)	0.013 ± 0.002	0.012 ± 0.002	0.001	0.06	0.83	0.42 to 0.98	7.56

*indicates significance at $p < 0.05$),

intraclass correlation coefficient (ICC), 95% confidence interval (CI), and coefficient of variation (CV)

Table 3

Interocular measures for each animal (n = 8); right and left eyes are compared with paired t-test

	OD	OS	Difference	p value	ICC	95% CI	CV (%)
Total retinal thickness (μm)	150.51 ± 8.45	151.75 ± 5.10	1.24	0.55	0.80	0.02 to 0.96	2.66
GC/NFL thickness (μm)	39.13 ± 5.71	41.65 ± 2.69	2.52	0.17	0.62	−0.92 to 0.92	11.15
Outer retinal thickness (μm)	70.29 ± 3.13	68.59 ± 3.24	1.70	*0.02	0.93	0.64 to 0.99	2.35
Choroidal Thickness (μm)	74.76 ± 8.75	69.77 ± 11.46	4.99	0.23	0.62	−0.89 to 0.92	11.76
BMO area (mm^2)	0.183 ± 0.017	0.196 ± 0.014	0.011	0.15	0.44	−1.80 to 0.89	8.16
BMO diameter (μm)	482.70 ± 22.28	496.62 ± 18.31	13.92	0.15	0.42	−1.88 to 0.88	4.02
MRW (μm)	140.34 ± 22.32	138.34 ± 18.45	2.0	0.22	0.69	−0.53 to 0.94	11.40
Rim Volume (mm^3)	0.0127 ± 0.0032	0.0127 ± 0.0016	6.15×10^{-5}	0.95	0.63	−0.85 to 0.93	16.51

*indicates significance at $p < 0.05$),

intraclass correlation coefficient (ICC), 95% confidence interval (CI), and coefficient of variation (CV)

Table 4

Intersession measures for the left eye of each animal (n = 9), sessions compared with paired t-test

	Session 1	Session 2	Difference	p value	ICC	95% CI	CV (%)
Total retinal thickness (μm)	152.29 ± 5.04	152.26 ± 6.01	0.03	0.96	0.96	0.84 to 0.99	0.90
GC/NFL thickness (μm)	41.72 ± 2.52	42.28 ± 3.31	0.56	0.22	0.95	0.78 to 0.99	2.17
Outer retinal thickness (μm)	68.32 ± 2.75	68.37 ± 3.09	0.05	0.92	0.93	0.67 to 0.98	1.50
Choroidal Thickness (μm)	70.5 ± 10.93	71.38 ± 10.55	0.88	0.52	0.97	0.85 to 0.99	4.17
BMO area (mm^2)	0.192 ± 0.023	0.189 ± 0.018	0.002	0.79	0.46	−1.39 to 0.88	10.23
BMO diameter (μm)	493.79 ± 31.89	490 ± 24.07	2.81	0.81	0.44	−1.50 to 0.87	4.96
MRW (μm)	130.43 ± 15.64	137.23 ± 17.57	6.80	0.08	0.90	0.55 to 0.98	6.08
Rim Volume (mm^3)	0.0126 ± 0.0022	0.0126 ± 0.0013	3.3×10^{-6}	0.99	0.88	0.47 to 0.97	6.98

*indicates significance at $p < 0.05$),

intraclass correlation coefficient (ICC), 95% confidence interval (CI), and coefficient of variation (CV)

Table 5

Measures derived from OCT imaging and histology for the same eyes (n = 7)

Variable (μm)	OCT	Histology	Difference	r	p value
Total retinal thickness	151.17 ± 8.16	140.41 ± 10.57	10.76	0.65	0.11
GC/NFL thickness	39.49 ± 6.14	52.84 ± 10.29	13.34	0.58	0.17
Outer Retina thickness	70.26.32 ± 1.98	60.28 ± 8.42	9.99	0.29	0.53
Choroid thickness	69.82 ± 6.36	62.47 ± 1.13	7.35	−0.17	0.72